Journal of Advanced Ceramics
2023, **12**(8): 1521–1532
https://doi.org/10.26599/JAC.2023.9220769
ISSN 2226-4108
CN 10-1154/TQ

Research Article

Microwave characterization of two $Ba_{0.6}Sr_{0.4}TiO_3$ dielectric thin films with out-of-plane and in-plane electrode structures

Hanchi Ruan[a], Theo Graves Saunders[a], Henry Giddens[a], Hangfeng Zhang[b], Achintha Avin Ihalage[a], Jonas Florentin Kolb[a], Matthew Blunt[c], Sajad Haq[d], Haixue Yan[b,*], Yang Hao[a,*]

[a]*School of Electronic Engineering and Computer Science, Queen Mary University of London, London E1 4NS, UK*
[b]*School of Engineering and Materials Science, Queen Mary University of London, London E1 4NS, UK*
[c]*Department of Chemistry, University College London, London WC1H 0AJ, UK*
[d]*Advanced Services and Products, QinetiQ, Farnborough GU14 0LX, UK*

Received: February 28, 2023; Revised: April 28, 2023; Accepted: May 18, 2023

Abstract: Ferroelectric (FE) thin films have recently attracted renewed interest in research due to their great potential for designing novel tunable electromagnetic devices such as large intelligent surfaces (LISs). However, the mechanism of how a polar structure in the FE thin films contributes to desired tunable performance, especially within the microwave frequency range, which is the most widely used frequency range of electromagnetics, has not been illustrated clearly. In this paper, we described several straightforward and cost-effective methods to fabricate and characterize $Ba_{0.6}Sr_{0.4}TiO_3$ (BST) thin films at microwave frequencies. The prepared BST thin films here exhibit homogenous structures and great tunability (η) in a wide frequency and temperature range when the applied field is in the out-of-plane direction. The high tunability can be attributed to high concentration of polar nanoclusters. Their response to the applied direct current (DC) field was directly visualized using a novel non-destructive near-field scanning microwave microscopy (NSMM) technique. Our results have provided some intriguing insights into the application of the FE thin films for future programmable high-frequency devices and systems.

Keywords: ferroelectric (FE); microwave; tunability; polarization; thin film

1 Introduction

Tunable electromagnetics has been proven to be vital for new emerging applications including active metasurfaces, coding metamaterials, and large intelligent surfaces (LISs), which will play an important role in future generations of wireless communication including software-defined radios (SDRs). Nonlinear dielectric materials are promising candidates for a variety of enhanced tunability (η) as the permittivity of these materials can be adjusted or "tuned" with the application of external stimuli such as an applied electric field [1]. Thus, the amplitude and phase of electromagnetic waves can be manipulated for both transmission and reflection [1,2]. These capabilities

* Corresponding authors.
E-mail: H. Yan, h.x.yan@qmul.ac.uk;
Y. Hao, y.hao@qmul.ac.uk

allow the design of tunable devices such as resonators [3], transmission lines [4], filters [5], varactors, and phase shifters [6] for spectral and temporal control of radio signals, leading to the development of a novel architecture in the generation after next (GAN) wireless communications. Thus, there have been increasing demands for novel material discovery and optimization, including those nonlinear ferroelectric (FE) materials with high dielectric tunability, low loss tangents ($\tan\delta$), and large figures of merit (FOMs).

The FE materials are well-known for their strong nonlinear response to an applied electric field, either in their paraelectric (PE) phase or FE phase. In the past decade, FEs have always been studied in either bulk or film for tunable microwave applications. However, bulk FEs face major drawbacks such as the requirement of high tuning voltages and large sizes of devices, which are not ideal for miniaturization and integration of communication devices. These disadvantages can be alleviated by replacing them with FE thin films, wherein the required electric field is generated at a fraction of the voltage needed for the bulk FEs. Besides, FEs fabricated in the film configuration offer the means to integrate themselves onto high-frequency devices based on III–V semiconductors.

The main application of tunable FE thin films for wireless communications is using them as tunable electronic components for beam steering antennas. The beam steering antennas can formulate lower side lobes of narrow directional beams to be steered in an appropriate direction of transmission and reception [7]. This technique has many merits, including producing higher directivity and gain, reduction in interference by avoiding interfering signals and directing the beam in the required direction, and capability of power-saving. Such beam steering antennas have a substantially broad military and commercial use including wireless networking and radar systems. The beam steering can be achieved by changing the phase of the input signal on all radiating elements. The PE phase of $Ba_{0.6}Sr_{0.4}TiO_3$ (BST) thin films is used to realize tunable varactors for achieving electronic beam steering. Since the permittivity of the BST thin films in their PE phase can be changed monolithically under the applied direct current (DC) bias, which can help change the phase of the input signal. Besides, the BST thin films are capable of continuous tuning at very high speeds with consuming low DC power [8].

Both dielectric permittivity (ε') and $\tan\delta$ of FE are temperature dependent. Generally, the FE material has a phase transition that happens at Curie point (T_C) [9]. Above T_C, the FE material is in its PE phase [1,10] and exhibits dielectric nonlinearity due to the existence of isolated local dipoles near T_C. Recently, these isolated local dipoles are defined as polar nanoclusters, which are embedded within a non-polar cubic matrix [11,12]. This structure could avoid domain switching that causes high loss at the FE phase below T_C. Therefore, the FE materials are always desired to be used in their PE phase for tunable applications.

One of the most intensively studied FE compositions for tunable microwave applications is barium strontium titanate ($Ba_xSr_{1-x}TiO_3$), which is a solid solution compound that exhibits PE or FE properties at room temperature, depending on the specific composition [1,12]. Normally, T_C of the FE thin film and ceramic bulk are different, even though they have the same composition because there is an effect from the substrate in the film fabrication process [13,14]. We have selected the composition of BST because its T_C in the form of the ceramic bulk is below room temperature, and it is not a relaxor FE, which enables us to prepare the film with high tunability and low loss [12,15]. Moreover, we have provided a straightforward and convenient method to characterize the tunable dielectric properties of the FE thin films in the microwave frequency range and the wide temperature range, which are important regarding tunable material research. Furthermore, we have first highlighted the difference between out-of-plane tuning and in-plane tuning using two different structured BST thin films for different applications. This also helps to understand how to achieve high tunability from the FE thin films through the appropriate tuning direction.

The BST thin films were prepared through the sol–gel and spin-coating soft chemistry processes, grown on two different substrates, namely $Pt/Ti/SiO_2/Si$ and sapphire, respectively. The BST thin film grown on the $Pt/Ti/SiO_2/Si$ substrate (abbreviated as BST/$Pt/Ti/SiO_2/Si$) can be coated with a top parallel plate electrode to work as a varactor through out-of-plane electrical tuning. Our fabricated BST/$Pt/Ti/SiO_2/Si$ demonstrates large tunability of over 50% in the frequency range from 1 to 5 GHz. The BST thin film grown on the sapphire substrate (abbreviated as BST/sapphire) can be patterned and used as a tunable coplanar waveguide (CPW) through in-plane electrical tuning. We developed CPW on this BST/sapphire film

surface for measurement, which shows constant tunability of 15% at microwave frequencies from 1 to 8 GHz. Both BST/Pt/Ti/SiO_2/Si and BST/sapphire can work as tunable elements in RF ends for achieving phase shifting or beam steering to improve wireless communication systems [16,17], depending on the requirement of different applications. To simplify the electrode patterning process, an approach of using a magnetic mask was developed to deposit the required pattern on the surface of the BST thin films, which opens possibility for low-cost and high-throughput material characterization at high microwave frequencies. Finally, the distributions of the electric field in these two films are illustrated clearly to explain why they exhibit different tunable performance and provide insights into how the electrode configuration affects the tunability of the BST thin films at the microwave frequencies.

2 Materials and methods

2. 1 Preparation of precursor solution

BST precursor solution was synthesized using barium acetate, strontium acetate, and titanium(IV) isopropoxide as starting materials. Stoichiometric amounts of barium acetate and strontium acetate were mixed in acetic acid. The solution was heated at 70 ℃ and stirred for 40 min to dissolve all particles. Then a stoichiometric amount of titanium(IV) isopropoxide was added to the solution, and the solution was stirred at 70 ℃ for another 30 min. To this solution, ethylene glycol was added in 1 : 3 proportion to acetic acid. The sol thus prepared was stirred for 1 h for complex formation at 90 ℃ to obtain stoichiometric, transparent, and stable precursor solution. The concentration of the final solution was adjusted to 0.3 M with solution at a 1 : 3 ratio of ethylene glycol : acetic acid.

2. 2 Film preparation

The pure BST precursor solution was deposited on a Pt/Ti/SiO_2/Si substrate by spin-coating at 3000 $r \cdot min^{-1}$ for 30 s to form a single layer. After each spin-coating cycle, the film sample was dried in air at 250 ℃ for 5 min on a hot plate, and then it was pyrolyzed at 500 ℃ for 10 min in a Lenton tube furnace to remove any organic contamination inside the film. This procedure was repeated 6 times to obtain the BST thin film with desired thickness. Finally, the pre-baked films were crystallized by annealing in air at 700, 750, and 800 ℃ for 60 min. Among these three BST thin films, the film sintered at 750 ℃ demonstrated the densest microstructure and best tunable performance, as shown in Figs. S1–S4 in the Electronic Supplementary Material (ESM). Then the same fabrication process was used to prepare the BST thin film grown on a sapphire substrate, and the film was sintered at 750 ℃.

2. 3 Film characterization

Structural properties including crystalline structures of the BST thin films were investigated by the X-ray diffraction (XRD) measurement. XRD data were collected on an X-ray diffractometer (X'Pert Pro, PANalytical) fitted with a detector (X'Celerator, PANalytical) using Ni-filtered Cu-Kα radiation ($\lambda = 1.5418$ Å). The BST thin film was coated with gold (Au) for surface and cross-sectional morphology characterization by a scanning electron microscope (SEM; Inspect-F Oxford, FEI) operated at 10 kV.

For dielectric measurements below 1 MHz, an Au top circular electrode with a diameter of 0.4 mm was deposited on the surface of BST/Pt/Ti/SiO_2/Si using a sputter coater (SC7620, EMITECH) through a designed mask. The top Au electrode, BST thin film, and bottom platinum (Pt) electrode together form a metal–dielectric–metal (MDM) capacitor. A precision impedance analyzer (4294A, Agilent) was used to measure dielectric permittivity, tunability, and $\tan\delta$ of it over the frequency range from 1 kHz to 1 MHz and the temperature range from 10 to 50 ℃ by connecting it with a sample stage, whose temperature can be controlled and adjusted. Temperature-dependent dielectric properties in a wider temperature range from −80 to 140 ℃ were measured with an LCR meter (4284A, Agilent). Polarization–electric (*P*–*E*) field and current–electric (*I*–*E*) field loops were measured by an FE hysteresis measurement tester (NPL) with the voltage applied in the triangular waveform at 10 Hz [18]. An atomic force microscope (AFM; 5600LS, Agilent) was connected with a network analyzer (N5231A PNA-L, Agilent) to conduct near-field scanning microwave microscopy (NSMM) measurement.

For the microwave characterization of the BST/Pt/Ti/SiO_2/Si sample, a silver parallel plate electrode was patterned on the surface of the BST film to form a parallel plate varactor for measurement. Each electrode

was patterned as a central circular patch surrounded by a concentric electrode on the measured FE thin film following the structure, as shown in Figs. 1(a) and 1(b). Two central patches with different radii of $20\sqrt{2}$ and $20\sqrt{3}$ μm were patterned on the same BST thin film, and then used for measurement to remove parasitic effect for extraction of their dielectric properties. Another smaller central patch with a radius of 20 μm was also patterned on the same sample to measure the reflection parameter (S_{11}) within a wider frequency range. These three central patches were all surrounded by the same concentric electrode, which was patterned as a ring shape with an inner radius of 80 μm and an outer radius of 300 μm.

For the microwave characterization of the BST/sapphire sample, the dielectric properties of the BST thin film were measured from CPW, which was made up of Au and deposited on the surface of the BST thin film. As shown in Fig. 1(c), the CPW pattern with transition was patterned on the surface of BST/sapphire and used for measuring this sample at the microwave

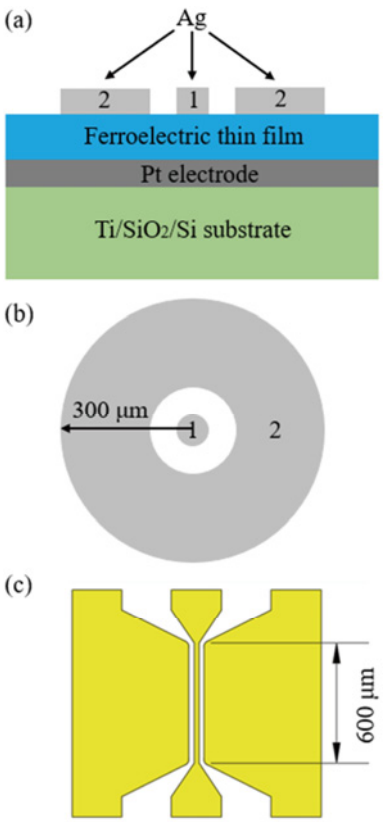

Fig. 1 (a) Cross-sectional and (b) top view of parallel plate varactor. (c) Top–down image of CPW pattern (transmission line with transition) used for measuring dielectric permittivity and tunability of BST thin film grown on sapphire substrate.

frequencies. CPW consists of a center conductor, separated from two ground planes by gaps. In the middle straight transmission line, the widths of the center conductor and the ground plane are 50 and 200 μm, respectively. The gap between the center conductor and the ground plane is 25 μm, and the length of this part is 600 μm. The transition parts at the top and bottom in this pattern allow probes with a larger tip gap for landing to avoid a short circuit happening at the gap between tips of the probe when applying a higher voltage.

For patterning the parallel plate electrode on the BST/Pt/Ti/SiO_2/Si sample and CPW on the BST/sapphire sample, a robust approach was developed by depositing silver or Au on the film surface through a designed magnetic mask using a sputter coater (AGB7341, Agar Auto). The mask is made of 430 stainless steel, which is the magnetic material, and thus it can be attracted by a magnetic holder underneath the BST thin film sample. In this way, the magnetic stainless steel mask, BST thin film sample, and magnetic holder could form a sandwich structure for sputter coating. The magnetic force between the mask and the holder is nearly even, which can help get the required pattern coated on the film surface.

After coating the required pattern, the one-port reflection measurement (for a parallel plate electrode on BST/Pt/Ti/SiO_2/Si) or two-port transmission measurement (for CPW on BST/sapphire) at the microwave frequencies was carried out by a network analyzer (N5230C PNA-L, Agilent) with applying different DC voltages. The scattering parameters (*S* parameters) were recorded for further data extraction. A 100 μm ground–signal–ground RF probe (model number: 40M-GSG-100-PLL, GGB Industries) or a pair of 525 μm ground–signal–ground RF probes (model number: 40M-GSG-525-PLL-OPT5, GGB Industries) was connected with PNA-L and used to land on the parallel plate electrode or CPW electrode; correspondingly, for one-port reflection measurement or two-port transmission measurement, a bias-tee (model number: SB18D3D, SigaTek) was used to apply the DC bias.

3 Results and discussion

3.1 Phase structures and morphologies

XRD patterns of the BST films grown on the Pt/Ti/

SiO_2/Si substrate and sapphire substrate are shown in Fig. 2. The (100), (110), (111), (200), (210), and (211) peaks corresponded to a perovskite structure are all clearly shown in both samples without the second phase, which indicates that each fabricated film possesses a polycrystalline perovskite structure. XRD profiles of the two BST thin films grown on different substrates are both well-fitted with a cubic perovskite structure in the space group $Pm\bar{3}m$, as shown in Fig. S5 in the ESM. The calculated lattice constants and angles of the BST thin film grown on the Pt/Ti/SiO_2/Si substrate and sapphire substrate are shown in Table S1 in the ESM. The lattice constants of cubic Pt are $a = b = c = 3.924$ Å, while the lattice constants of sapphire are $a = b = 4.758$ Å. When the lattice constants of the deposited layer and the substrate are close, the lattice mismatch strain could induce lattice changes of the film. The lattice constant of the BST ceramic bulk is 3.965 Å, which is slightly higher than the lattice constant of Pt. Thus, a small lattice mismatch between the BST thin film and the Pt layer results in the compressed strain in the BST thin film, inducing decreased lattice constants of the BST thin film grown on the Pt/Ti/SiO_2/Si substrate. However, since the lattice mismatch between the BST thin film and the sapphire substrate is large, the lattice mismatch strain has less effect on the lattice constant of the BST thin film. This leads to the BST thin film being grown on the sapphire substrate with a lattice constant that is close to the BST ceramic bulk with the same composition [19].

Figure 3 shows a smooth surface without cracks and uniform thickness of the BST thin films grown on both

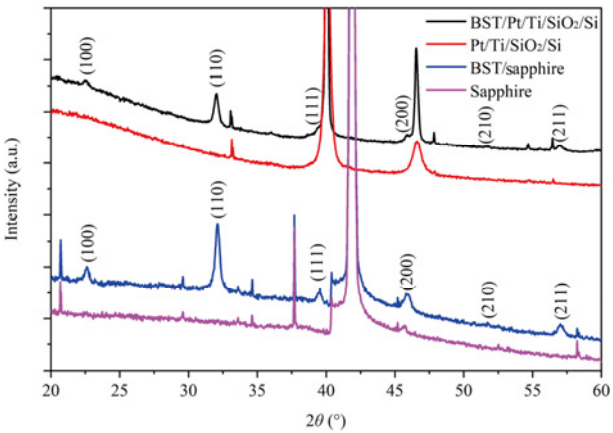

Fig. 2 XRD patterns of BST thin films grown on Pt/Ti/SiO_2/Si substrate or sapphire substrate. The main reflections of perovskite phase are indexed. XRD patterns of Pt/Ti/SiO_2/Si substrate and sapphire substrate are added for reference.

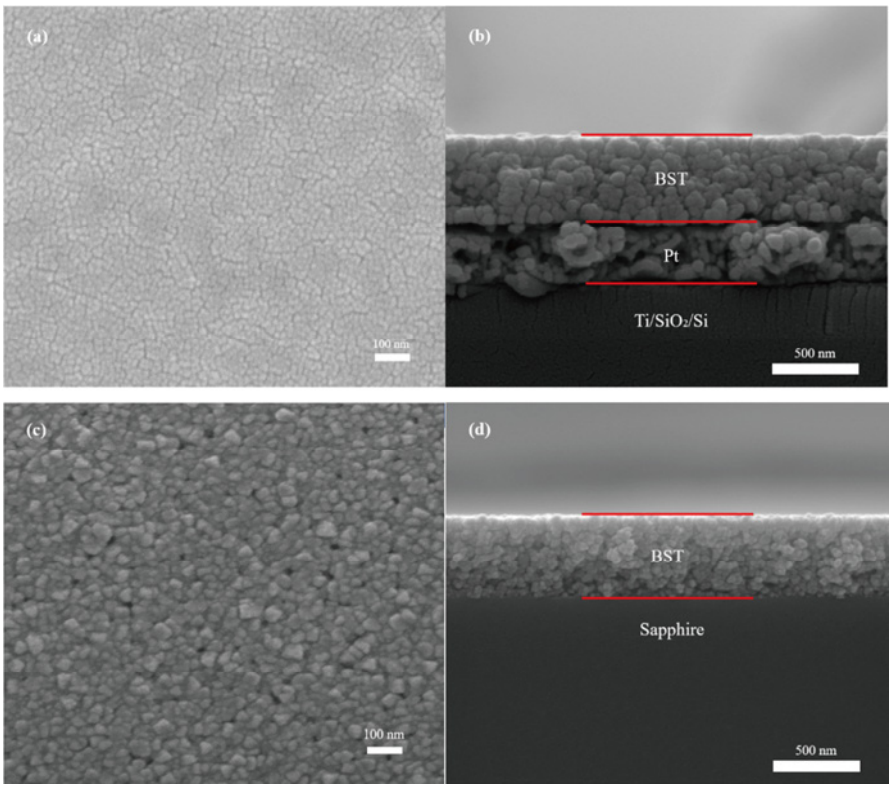

Fig. 3 Surface and corresponding cross-sectional SEM images of BST thin film. (a, b) BST thin film grown on Pt/Ti/SiO_2/Si substrate. (c, d) BST thin film grown on sapphire substrate.

substrates. The average grain sizes of the BST thin film grown on the Pt/Ti/SiO_2/Si substrate and the sapphire substrate were calculated as 13.83 and 24.66 nm, respectively, using the software of ImageJ. The distributions of the grain size, with their calculated average grain sizes and standard deviations of each BST thin film, can be seen in Fig. S6 in the ESM. High-resolution cross-sectional SEM images of these two BST thin films are shown in Fig. S7 in the ESM, and they reveal no secondary layer between the BST thin film and its corresponding substrate.

3. 2 Dielectric properties

3.2.1 BST/Pt/Ti/SiO_2/Si

Thermal dependency of the dielectric permittivity of the BST thin film grown on the Pt/Ti/SiO_2/Si substrate at 10, 100, and 500 kHz are shown in Fig. S8 in the ESM. The BST thin film exhibits a broadened phase transition from the FE phase to the PE phase with the transition temperature between −49.0 and −34.3 ℃. While above this phase transition, it transfers to a nominally PE phase and contains polar nanoclusters embedded within a non-polar cubic matrix [12]. Each polar nanocluster contains switchable dipoles, and the polarization contribution to the dielectric permittivity intrinsically originates from dipole rotation [11,20]. It is very difficult to directly observe the polar nanoclusters using typical high-resolution microscopy [11,21]. However, the presence of the polar nanoclusters was also indicated by PE nature confirmed by dielectric test and polarization change under the voltage [22,23], which act as the signature of the polar nanoclusters.

Figure S9 in the ESM shows *P*–*E* and *I*–*E* loops of the BST thin film measured under different applied electric fields at 10 Hz. In the *I*–*E* loops, the peaks near the *y*-axis indicate a rotation of the polar nanoclusters in the PE phase under the applied voltage. Both *P*–*E* and *I*–*E* loops are asymmetric since the BST thin film was coated with different bottom electrodes and top electrodes, which are Pt and Au, respectively, to form a MDM structure. This symmetry breaking could cause poling effect at the electrode–FE interface [24]. In this case, the impact of nonidentical electrodes is similar to that of an external DC bias field. This could result in a smearing of dielectric anomaly [25,26], which also leads to a broadened phase transition peak, as shown in Fig. S8 in the ESM.

Meanwhile, there is an interfacial dielectric layer between the BST thin film and the Pt layer, which is commonly called as the “dead layer” [27] and also contributes to asymmetric shapes of the *P*–*E* and *I*–*E* loops. Besides, since this “dead layer” shows much lower dielectric permittivity than the BST thin film and forms a parasitic capacitor in series with the film [28], the measured dielectric permittivity of the BST thin-film capacitor is reduced compared to that of the BST bulk sample. In addition, the grain size of the BST thin film is much smaller than that of the BST bulk (normally above 1 μm), which also causes lower dielectric permittivity of the BST thin film compared with that of the BST bulk. Since the smaller grain size would lead to more grain boundaries inside the thin film, the dielectric permittivity of the grain boundaries is much lower than that of the grain, causing lower overall dielectric permittivity of the BST thin film.

Figures 4(a) and 4(b) show variations of ε' and $\tan\delta$ of the BST thin film in the frequency range from 1 kHz to 1 MHz at 25 ℃ without the bias and with the applied DC electric field of 30 kV·mm^{-1}, respectively. These results were all obtained by applying an oscillation voltage of 0.5 V. The film thickness characterized by SEM is 500 nm, and a low DC bias voltage of 15 V was applied in this test, resulting in the applied electric field of 30 kV·mm^{-1}. The dielectric response results from a short-range rotation of dipoles under the influence of an externally applied electric field. The dielectric permittivity of the BST thin film gradually decreases when the DC bias is increasing, leading to dielectric tunability. The η of a material can be expressed by Eq. (1):

$$\eta = \frac{\varepsilon_0 - \varepsilon_E}{\varepsilon_0} \times 100\% \quad (1)$$

where ε_0 and ε_E are the dielectric permittivity at zero and applied field, respectively.

Figures 4(a) and 4(b) also show that the dielectric permittivity and $\tan\delta$ of the BST film both decrease in the whole measured frequency range when applying the DC field. Under the applied electric field of 30 kV·mm^{-1}, high tunability of 60.2% at 1 MHz and 25 ℃ is obtained. For tunable microwave devices, FOM is always chosen to qualify tunable performance, which is defined as FOM = tunability/$\tan\delta$. Table 1 compares the dielectric properties of the BST thin films prepared in this work with those reported in Refs. [29–33]. The BST thin film grown on the Pt/Ti/SiO_2/Si substrate from this work exhibits superior tunability

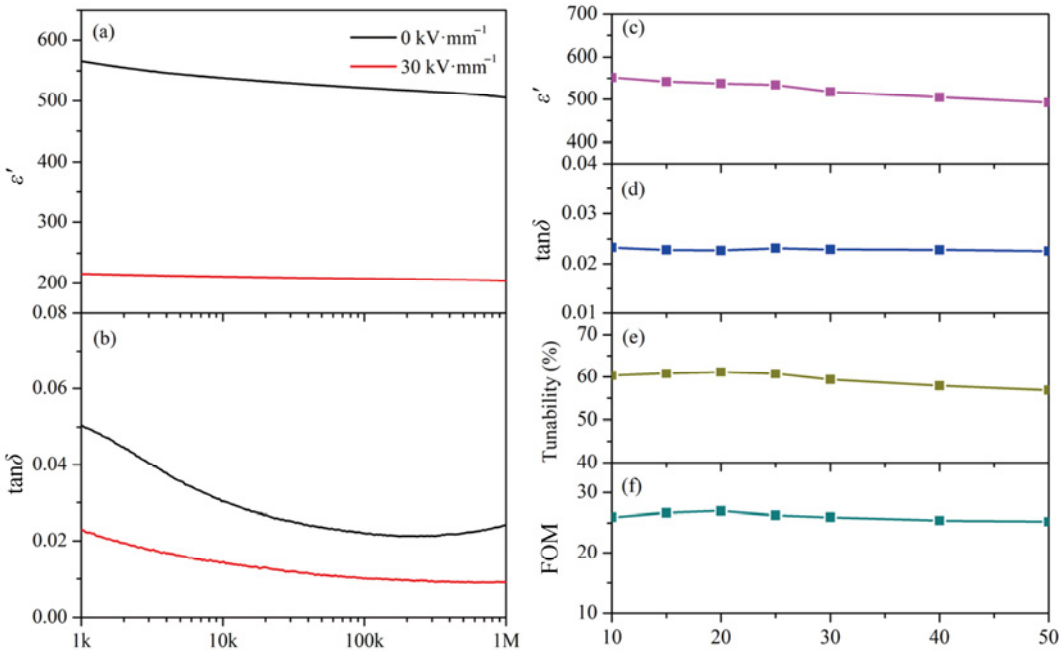

Fig. 4 (a) ε' and (b) tanδ of BST thin film grown on Pt/Ti/SiO_2/Si substrate without bias and with applied DC electric field of 30 kV·mm^{-1} (DC bias of 15 V) from 1 kHz to 1 MHz at 25 ℃. (c) ε' and (d) tanδ of BST thin film grown on Pt/Ti/SiO_2/Si substrate without bias from 10 to 50 ℃ at 100 kHz. (e) Tunability and (f) FOMs of BST thin film grown on Pt/Ti/SiO_2/Si substrate under electric field of 30 kV·mm^{-1} in temperature range of 10–50 ℃ at 100 kHz.

Table 1 Dielectric properties of BST thin films prepared in this work in comparison with those reported in Refs. [29–33]

Material	Preparation method	Frequency	Tunability (%)	Loss	FOM
BST (this work)	Sol–gel	100 kHz	60.2 (30 kV·mm^{-1})	0.0220	27.4 (30 kV·mm^{-1})
BST [29]	Sol–gel	100 kHz	34.2 (50 kV·mm^{-1})	0.0250	13.7 (50 kV·mm^{-1})
BST [30]	Sol–gel	100 kHz	65.3 (50 kV·mm^{-1})	0.0618	10.6 (50 kV·mm^{-1})
BST [31]	Sol–gel	2 MHz	46.53 (37.7 kV·mm^{-1})	0.0184	25.3 (37.7 kV·mm^{-1})
BST [32]	Magnetron sputtering	100 kHz	49.4 (45.5 kV·mm^{-1})	0.0150	32.9 (45.5 kV·mm^{-1})
BST [33]	Pulsed laser deposition	10 kHz	48.5 (30 kV·mm^{-1})	0.0280	17.3 (30 kV·mm^{-1})

and FOM values, achieved through a cost-effective and efficient technique.

As shown in Fig. S8 in the ESM, at 25 ℃, the film is above and close to the phase transition range. Thus, the dipoles inside are active under the DC bias at this status, resulting in high tunability. Table S2 in the ESM also indicates that as the applied electric field is increasing, the dielectric permittivity and tanδ gradually decrease, while the tunability gradually increases. The reason is that when applying the DC field, the original dipole direction will rotate towards the direction of the DC bias, and the activity of the dipoles in the BST thin film is restrained by the applied DC bias field in this way, resulting in lower dielectric permittivity and lower tanδ [34].

Figures 4(c)–4(f) show temperature-dependent tunable performance of the BST thin film in the temperature range of 10–50 ℃ and at the frequency of 100 kHz. In Fig. 4(e), the tunability increases from 10 to 20 ℃, and then decreases from 20 to 50 ℃. As shown in Figs. 4(e) and 4(f), the highest tunability and highest FOM value of the BST thin film, respectively, can be obtained in the temperature range from 15 to 25 ℃, which is around the room-temperature range. Further increasing the temperature above T_C results in reducing the density of the polar nanoclusters. At the same time, the dipoles inside the polar nanoclusters become more active and exhibit better flexibility since they have more energy to rotate at a higher temperature, which can lead to higher tunability. Thus, when increasing the temperature from T_C, lower concentration of the polar nanoclusters and more active dipoles reach a trade-off from 15 to 25 ℃, generating the highest tunability and FOM in this temperature range.

The ε' and $\tan\delta$ of the prepared BST thin film grown on the Pt/Ti/SiO_2/Si substrate in the microwave frequency range of 1–5 GHz without an applied DC bias are shown in Figs. 5(a) and 5(b), respectively, which were extracted from measured S_{11} of the sample following the extraction method described in Ref. [35]. The ε' decreases significantly from 516.9 at 1 MHz to 68.4 at 1 GHz, and it keeps decreasing to 54.7 at 5 GHz. It is because in the dielectric material, there are different types of polarization mechanisms, and each of them works at different frequencies [20,36]. The dipoles with shorter relaxation time could contribute to the polarization and dielectric permittivity at both low and high frequencies, while the dipoles with longer relaxation time only contribute to the dielectric permittivity at low frequencies [12].

Figure 5(c) shows the tunability of the BST thin film in the frequency range from 1 to 5 GHz under 50 kV·mm^{-1} (an applied DC bias of 25 V). It demonstrates the high tunability above 50% in the whole frequency range under the low applied voltage. However, it is lower than the tunability of 60.2% at 1 MHz, which is achieved from the same film and under an even lower applied electric field of 30 kV·mm^{-1}. This is also due to less polarization that exists in the BST thin film in the higher frequency range. Thus, when applying the DC bias, there are fewer dipoles that could rotate toward the direction of the electric field, resulting in lower tunability.

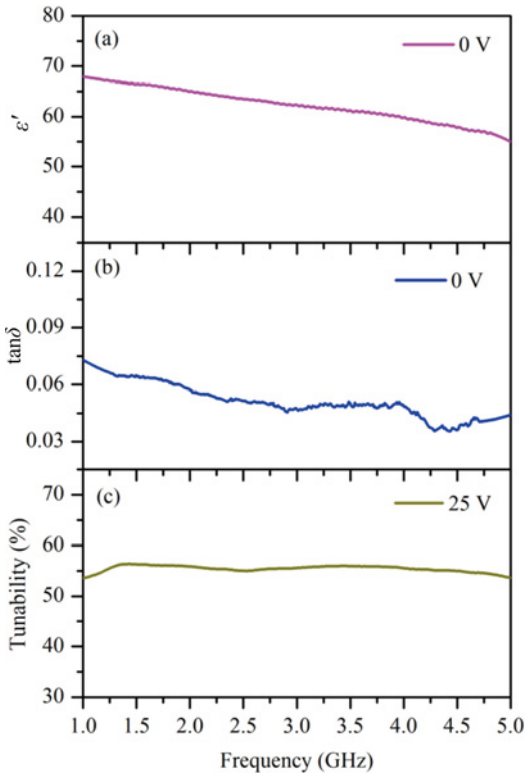

Fig. 5 (a) ε' and (b) tanδ of BST thin film grown on Pt/Ti/SiO_2/Si substrate without bias at 1–5 GHz at 25 ℃. (c) Tunability of BST thin film grown on Pt/Ti/SiO_2/Si substrate under 25 V (electric field of 50 kV·mm^{-1}) in frequency range from 1 to 5 GHz at 25 ℃.

NSMM is one of the innovative tools used to study bulks, thin films, and nanoscale materials and devices. The goal of NSMM is to bring quantitative broadband measurements at the microwave frequencies down to micrometer or nanometer levels [37]. For tunable materials, the permittivity of the material changes when a DC bias is applied, leading to different impedance and consequently different S_{11}. The NSMM technique can be used to visualize the change in S_{11} of the sample under the applied DC bias in the microwave frequency range, providing a direct way to observe the tunable region of the sample. To further study how the local area inside the BST film acts under a DC bias, the BST/Pt/Ti/SiO_2/Si sample was characterized by NSMM. The low voltage of 10 V was applied on the BST thin film at 6.7 GHz by voltage biasing the probe tip. The grounded Pt beneath the dielectric thin film acts as a ground plane. As shown in Fig. S10 in the ESM, in the NSMM image of 400 μm^2 area, there are changes in the signal from the S_{11} phase in different small areas under 10 V.

The data measured from NSMM need to be processed to compare the phase difference and topography difference without bias and under the bias of 10 V to remove topography effect on the S_{11} change under the applied bias. As can be seen in Fig. 6, both mappings are min–max normalized to allow the comparison between the two measured quantities. We investigated whether the tunability has any dependence on topography (roughness) of the sample by calculating the two-dimensional (2D) correlation coefficient (r) between the normalized phase and the topography difference mappings (Eq. (2)) [38]:

$$r = \frac{\sum_m \sum_n (P_{mn} - \bar{P})(T_{mn} - \bar{T})}{\sqrt{\left[\sum_m \sum_n (P_{mn} - \bar{P})^2\right]\left[\sum_m \sum_n (T_{mn} - \bar{T})^2\right]}} \quad (2)$$

where P_{mn} indicates the phase difference at the (m,n)th location (pixel) of the phase mapping (Fig. 6(a)), and $\bar{P}$ is the mean pixel intensity. Likewise, T_{mn} and $\bar{T}$ are the topography difference at the (m,n)th location

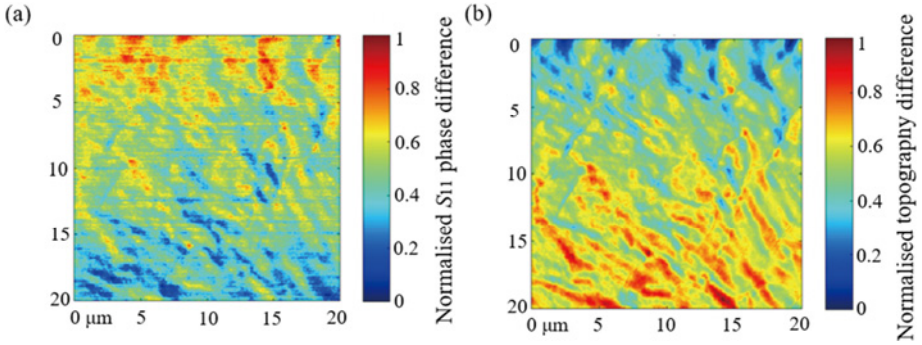

Fig. 6 (a) Difference of S_{11} phase measurements at 0 and 10 V DC biases, normalized to the range of 0–1. (b) Difference of topography measurements at 0 and 10 V DC biases, normalized to the range of 0–1. Both mappings have a pixel size of 256 × 256.

and the mean pixel intensity of the topography mapping (Fig. 6(b)), respectively. Both m and n run from 1 to 256. The r ranges from −1 to 1, and the sign of r reflects a negative or positive correlation, while 0 reflects no correlation at all between the two quantities. The calculated r between the measured phase difference and the topography difference mappings is 0.0412, indicating that the change of the S_{11} phase under a bias of 10 V has almost no dependence on the sample topography. This indicates that the change of the S_{11} phase from local areas inside the BST thin film contributes to the overall change of S_{11}, which represents the origin of the tunability.

Another evidence is that measured S_{11} of the BST/Pt/Ti/SiO_2/Si sample, which is the same sample, as characterized by NSMM, shows a clear shift under a DC bias of 10 V (an electric field of 20 kV·mm^{-1}) from 1 to 8 GHz, as shown in Fig. S11 in the ESM, which corresponds to the NSMM measurement and evidences the tunable performance. The phase of S_{11} increased when a DC bias of 10 V was applied since the capacitance of the BST-based varactor decreased under the bias. This material structure of the BST thin film grown on the conductive layer could be used for the tunable microwave device design such as the parallel plate varactor and phase shifters [39,40].

3.2.2 BST/sapphire

The CPW pattern was patterned on the surface of the BST/sapphire to measure and extract the dielectric permittivity and tunability of it at the microwave frequencies. CPW always acts as a transmission line for electromagnetic characterization at wideband frequencies. CPW was deposited onto both the surface of the reference sapphire substrate and the BST/sapphire for comparison and data extraction. The conformal mapping of the field within CPW was followed to determine the dielectric permittivity of the BST/sapphire thin film, following the procedures described in Refs. [41,42].

Figure 7 shows extracted ε' and tunability of the BST thin film grown on the sapphire substrate at 1–8 GHz. The ε' is decreasing from 144.9 at 1 GHz to 121.9 at 8 GHz due to fewer dipoles and polarization inside, while it is higher than that of the BST film grown on the Pt/Ti/SiO_2/Si substrate since the grain size of the BST grown on the sapphire is larger. Tunability data were obtained by applying a low voltage of 30 V through a GSG probe, and the tunability of around 15% was achieved in the whole frequency range of 1–8 GHz.

As can be seen in Fig. 8, when applying the same DC bias, the electric field generated by the parallel plate electrode is in the out-of-plane direction and applied fully through the BST thin film [39], while the

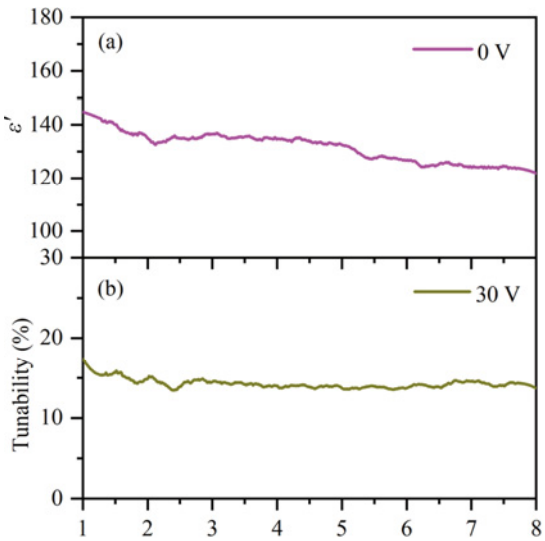

Fig. 7 (a) ε' without DC bias and (b) tunability of BST thin film grown on sapphire substrate under applied DC bias of 30 V as a function of frequency from 1 to 8 GHz.

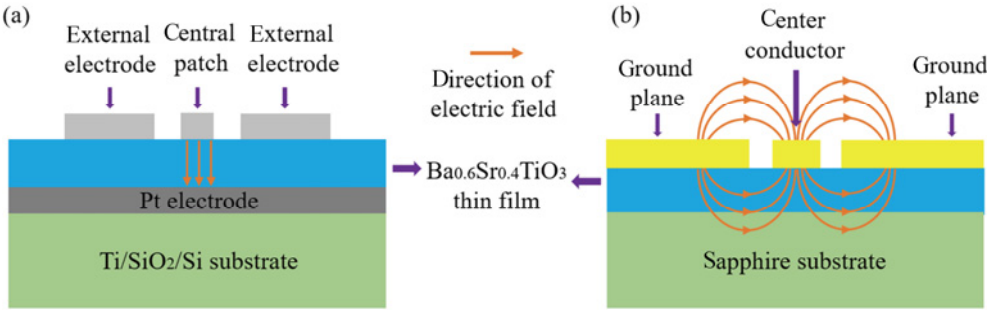

Fig. 8 Distributions of electric field following (a) out-of-plane direction in parallel plate electrode on BST/Pt/Ti/SiO_2/Si sample and (b) in-plane direction of CPW transmission line on BST/sapphire sample.

electric field applied by the CPW electrode is along the in-plane direction, and part of the DC electric field is going through the sapphire substrate other than the BST thin film [43]. Thus, the DC electric field generated by the parallel plate electrode could help lead to a much higher nominally electric field under the same DC bias voltage since the film thickness (500 nm) is much smaller than the gap width (25 μm) in the CPW electrode pattern. Therefore, the tunability obtained from BST/Pt/Ti/SiO_2/Si measured by the structure of the parallel plate varactor is higher than the tunability measured from BST/sapphire coated with the CPW electrode even though the applied DC voltage on the CPW electrode is higher.

4 Conclusions

In summary, BST thin films have been successfully fabricated on two different substrates of Pt/Ti/SiO_2/Si and sapphire by sol–gel and spin-coating soft chemistry methods, respectively. The dielectric properties and tunable performance of these two BST thin films have been explained clearly by the new concept of the presence of the polar nanoclusters inside the film.

For the BST/Pt/Ti/SiO_2/Si film, the high tunability and FOM value have been achieved around room temperature at 100 kHz since the phase transition of this film is near and below room temperature. Furthermore, the high tunability of over 50% has also been obtained in the microwave frequency range of 1–5 GHz from this BST thin film when integrating it as the parallel plate varactor. Meanwhile, the novel technique of NSMM was applied to observe the change of the S_{11} phase at the local area in the film under a DC bias, which could provide the evidence for the origin of the tunability of the BST thin film. For the BST/sapphire film patterned with the CPW transmission line for the microwave measurement, the tunability of around 15% has been achieved at 1–8 GHz, which could meet the requirement of the tunable microwave devices through in-plane tuning.

The distribution of the electric field plays an important role in tuning the BST thin films. These two BST thin films prepared on different substrates can be integrated with different electrode structures for various electrically tunable device designs.

Acknowledgements

We thank Mr. Anestis Katsounaros for providing instruction about the NSMM measurement. This work was supported by the "Software Defined Materials for Dynamic Control of Electromagnetic Waves" (ANIMATE) Project (QinetiQ IRAD Grant No. 41025673 and EPSRC Grant No. EP/R035393/1), and the authors acknowledge QinetiQ and Engineering and Physical Sciences Research Council (EPSRC). Hanchi Ruan acknowledges EPSRC for funding the Ph.D. studentship.

Declaration of competing interest

The authors have no competing interests to declare that are relevant to the content of this article. The author Haixue Yan is the Editorial Committee member of this journal.

Electronic Supplementary Material

Supplementary material is available in the online version of this article at https://doi.org/10.26599/JAC.2023.9220769.

References

[1] Ahmed A, Goldthorpe IA, Khandani AK. Electrically tunable materials for microwave applications. *Appl Phys Rev* 2015, **2**: 011302.

[2] Raveendran A, Sebastian MT, Raman S. Applications of microwave materials: A review. *J Electron Mater* 2019, **48**: 2601–2634.
[3] Wu L, Du T, Xu NN, *et al*. A new $Ba_{0.6}Sr_{0.4}TiO_3$–silicon hybrid metamaterial device in terahertz regime. *Small* 2016, **12**: 2610–2615.
[4] Rahman BMF, Divan R, Stan L, *et al*. Tunable transmission line with nanopatterned thin films for smart RF applications. *IEEE T Magn* 2014, **50**: 2801604.
[5] Schuster C, Wiens A, Schmidt F, *et al*. Performance analysis of reconfigurable bandpass filters with continuously tunable center frequency and bandwidth. *IEEE T Microw Theory* 2017, **65**: 4572–4583.
[6] Haghzadeh M, Armiento C, Akyurtlu A. All-printed flexible microwave varactors and phase shifters based on a tunable BST/polymer. *IEEE T Microw Theory* 2017, **65**: 2030–2042.
[7] Pradeep AS, Bidkar GA, Thippesha D, *et al*. Design of compact beam-steering antenna with a novel metasubstrate structure. In: Proceedings of the 2020 IEEE International Conference on Distributed Computing, VLSI, Electrical Circuits and Robotics, Udupi, India, 2020: 96–99.
[8] Karnati KK, Trampler ME, Gong X. A monolithically BST-integrated K_a-band beamsteerable reflectarray antenna. *IEEE T Antenn Propag* 2017, **65**: 159–166.
[9] Wang J, Lou J, Wang JF, *et al*. Ferroelectric composite artificially-structured functional material: Multifield control for tunable functional devices. *J Phys D Appl Phys* 2022, **55**: 303002.
[10] Shi PP, Tang YY, Li PF, *et al*. Symmetry breaking in molecular ferroelectrics. *Chem Soc Rev* 2016, **45**: 3811–3827.
[11] Bencan A, Oveisi E, Hashemizadeh S, *et al*. Atomic scale symmetry and polar nanoclusters in the paraelectric phase of ferroelectric materials. *Nat Commun* 2021, **12**: 3509.
[12] Zhang HF, Giddens H, Yue YJ, *et al*. Polar nano-clusters in nominally paraelectric ceramics demonstrating high microwave tunability for wireless communication. *J Eur Ceram Soc* 2020, **40**: 3996–4003.
[13] Bian YL, Zhai JW. Effects of CeO_2 buffer layer on the dielectric properties of $Ba_{0.6}Sr_{0.4}TiO_3$ thin films prepared by sol–gel processing. *J Sol–Gel Sci Techn* 2014, **69**: 40–46.
[14] Bian YL, Zhai JW. Low dielectric loss $Ba_{0.6}Sr_{0.4}TiO_3$/$MgTiO_3$ composite thin films prepared by a sol–gel process. *J Phys Chem Solids* 2014, **75**: 759–764.
[15] Feteira A, Sinclair DC, Reaney IM, *et al*. $BaTiO_3$-based ceramics for tunable microwave applications. *J Am Ceram Soc* 2004, **87**: 1082–1087.
[16] Yuan Y, Chen SJ, Fumeaux C. Varactor-based phase shifters operating in differential pairs for beam-steerable antennas. *IEEE T Antenn Propag* 2022, **70**: 7670–7682.
[17] Chen HW, Yang CR, Zhang JH, *et al*. High performance distributed CPW phase shifters with etched BST thin films on Φ 3″ $LaAlO_3$ substrates. *Solid State Sci* 2012, **14**: 117–120.
[18] Zhang M, Xu XZ, Ahmed S, *et al*. Phase transformations in an Aurivillius layer structured ferroelectric designed using the high entropy concept. *Acta Mater* 2022, **229**: 117815.
[19] Opel M. Spintronic oxides grown by laser-MBE. *J Phys D Appl Phys* 2012, **45**: 033001.
[20] Zhang M, Zhang HF, Jiang QH, *et al*. Terahertz characterization of lead-free dielectrics for different applications. *ACS Appl Mater Interfaces* 2021, **13**: 53492–53503.
[21] Yan R, Guo Z, Tai RZ, *et al*. Observation of long range correlation dynamics in $BaTiO_3$ near T_C by photon correlation spectroscopy. *Appl Phys Lett* 2008, **93**: 192908.
[22] Zhang HF, Gidden H, Saunders TG, *et al*. High tunability and low loss in layered perovskite dielectrics through intrinsic elimination of oxygen vacancies. *Chem Mater* 2020, **32**: 10120–10129.
[23] Liu ZK, Shang SL, Du JL, *et al*. Parameter-free prediction of phase transition in $PbTiO_3$ through combination of quantum mechanics and statistical mechanics. *Scripta Mater* 2023, **232**: 115480.
[24] Setter N, Damjanovic D, Eng L, *et al*. Ferroelectric thin films: Review of materials, properties, and applications. *J Appl Phys* 2006, **100**: 051606.
[25] Bratkovsky AM, Levanyuk AP. Smearing of phase transition due to a surface effect or a bulk inhomogeneity in ferroelectric nanostructures. *Phys Rev Lett* 2005, **94**: 107601.
[26] He Y, Li XM, Gao XD, *et al*. Tunable properties of LSCO buffered PMN–PT thin film capacitor. *Funct Mater Lett* 2011, **4**: 241–244.
[27] Yang Q, Cao JX, Zhou YC, *et al*. Dead layer effect and its elimination in ferroelectric thin film with oxide electrodes. *Acta Mater* 2016, **112**: 216–223.
[28] Liao JX, Yang CR, Zhang JH, *et al*. The interfacial structures of (Ba,Sr)TiO_3 films deposited by radio frequency magnetron sputtering. *Appl Surf Sci* 2006, **252**: 7407–7414.
[29] Kim KT, Kim CI. Electrical and dielectric properties of Ce-doped $Ba_{0.6}Sr_{0.4}TiO_3$ thin films. *Surf Coat Tech* 2006, **200**: 4708–4712.
[30] Liao JX, Xu ZQ, Wei XB, *et al*. Influence of preheating on crystallization and growing behavior of Ce and Mn doped $Ba_{0.6}Sr_{0.4}TiO_3$ film by sol–gel method. *Surf Coat Tech* 2012, **206**: 4518–4524.
[31] Luo W, Chen XY, Fan JW, *et al*. Effect of Rb-doping on the dielectric and tunable properties of $Ba_{0.6}Sr_{0.4}TiO_3$ thin films prepared by sol–gel. *Ceram Int* 2016, **42**: 17229–17236.
[32] Wang Y, Liu BT, Wei F, *et al*. Fabrication and electrical properties of (111) textured ($Ba_{0.6}Sr_{0.4}$)TiO_3 film on platinized Si substrate. *Appl Phys Lett* 2007, **90**: 042905.
[33] Qin WF, Zhu J, Xiong J, *et al*. Electrical behavior of Y-doped $Ba_{0.6}Sr_{0.4}TiO_3$ thin films. *J Mater Sci-Mater El* 2007, **18**: 1217–1220.
[34] Zheng Z, Yao YY, Weng WJ, *et al*. Dipole azimuth dependent permittivity in randomly and (100) oriented (Pb,Sr)TiO_3 thin films. *J Mater Chem* 2011, **21**: 10808–10812.

[35] Sheng S, Wang P, Zhang XY, *et al*. Characterization of microwave dielectric properties of ferroelectric parallel plate varactors. *J Phys D Appl Phys* 2009, **42**: 015501.
[36] Wilson JN, Frost JM, Wallace SK, *et al*. Dielectric and ferroic properties of metal halide perovskites. *APL Mater* 2019, **7**: 010901.
[37] Imtiaz A, Wallis TM, Kabos P. Near-field scanning microwave microscopy: An emerging research tool for nanoscale metrology. *IEEE Microw Mag* 2014, **15**: 52–64.
[38] Mohapatra S, Weisshaar JC. Modified Pearson correlation coefficient for two-color imaging in spherocylindrical cells. *BMC Bioinformatics* 2018, **19**: 428.
[39] Zhang XY, Wang P, Sheng S, *et al*. Ferroelectric $Ba_xSr_{1-x}TiO_3$ thin-film varactors with parallel plate and interdigital electrodes for microwave applications. *J Appl Phys* 2008, **104**: 124110.
[40] Annam K, Spatz D, Shin E, *et al*. Experimental verification of microwave phase shifters using barium strontium titanate (BST) varactors. In: Proceedings of the 2019 IEEE National Aerospace and Electronics Conference, Dayton, USA, 2020: 63–66.
[41] Carlsson E, Gevorgian S. Conformal mapping of the field and charge distributions in multilayered substrate CPWs. *IEEE T Microw Theory* 1999, **47**: 1544–1552.
[42] Ge JQ, Xia T, Wang GA. Design and optimization methodology of coplanar waveguide test structures for dielectric characterization of thin films. *J Electron Test* 2020, **36**: 183–188.
[43] Marksz EJ, Hagerstrom AM, Zhang XH, *et al*. Broadband, high-frequency permittivity characterization for epitaxial $Ba_xSr_{1-x}TiO_3$ composition-spread thin films. *Phys Rev Appl* 2021, **15**: 064061.